16th European Signal Processing Conference (EUSIPCO 2008), Lausanne, Switzerland, August 25-29, 2008, copyright by EURASIP

DIGITAL WAVEFIELD RECONSTRUCTION IN PHASE-SHIFTING HOLOGRAPHY AS INVERSE DISCRETE PROBLEM

Vladimir Katkovnik, Jaakko Astola, and Karen Egiazarian

Signal Processing Institute, Tampere University of Technology,
P.O. Box 553, Tampere, Finland. E-mail: firstname.lastname@tut.fi.

ABSTRACT

A novel discrete model for the wavefield propagation is proposed. This model is accurate (and aliasing free) for a pixel-wise constant object distribution which is invariant on rectangular elements of pixel's size of a digital hologram CCD sensor. The sizes of object and sensor arrays can be different. A spacial light modulator (SLM) is a good example of the object where a pixel-wise invariant distribution appears. We consider reconstruction of the object complex-valued distribution from the phase-shifting holography data as an inverse discrete problem. The reconstruction becomes more accurate when the sensor size is larger than the size of the object aperture. An efficient frequency domain algorithm is demonstrated.

1. INTRODUCTION

The wavefield reconstruction from intensity and phase measurements is one of the basic problems in digital wavefield imaging and holography in particular with application to high-accuracy measurements [1]. In most studies, a single wavelength is used to record a digital hologram where an image intensity and depth information is coded in a complex-valued wavefield distribution. Some of the standard reconstruction algorithms mimic the optical procedure when the hologram is illuminated with a reference beam. In discrete versions of these methods the recorded hologram is multiplied with the complex-valued distribution modeling the reference beam and the diffraction field is calculated.

In the phase-shifting holography, the complex-valued wavefield in the hologram plane is calculated from a few holograms recorded with different phase-shifts of the reference beam. Then another type of reconstruction algorithms can be used assuming that a complex-valued wavefield is already done in the hologram plane.

A contribution of this paper concerns a few aspects of digital modelling for optical wavefield propagation, reconstruction and design. A novel discrete diffraction transform (DDT) model of the wavefield propagation is presented in Section 3. This model is accurate for a pixel-wise invariant object distribution, i.e. for a distribution which is piece-wise constant on rectangular elements of pixel's size of the digital sensor. This discrete modelling gives accurate and aliasing free results for any pixel's size. Here we refer to the aliasing appearing as a result of discretization in the standard discrete approximations of the wavefield propagation integrals. This precise modelling of the wavefield propagation imitates an "ideal" physical experiment as it is presented by the integral propagation equations. In particular, this accurate modeling is useful for reliable design and computer testing of digital holography algorithms because these design and tests can be based on the precisely modelled observations. For an arbitrary continuous object distribution the proposed wavefield propagation modelling is approximate with the accuracy depending on the accuracy of the piece-wise fitting of the object wavefield distribution. In this case DDT continues to be accurate but for the piece-wise approximation of the object distribution. A spacial light modulator (SLM) generating a pixel-wise invariant wavefield distribution is a good example of the optical system where the developed digital modelling is relevant.

The frequency domain version of DDT is used for inverse reconstruction of the object wavefield distribution (Sections 4 and 5). The discrete propagation model introduced in this paper is a generalization to arbitrary sizes of object and image arrays of the model proposed in [2], where an equal size of the object and image arrays is assumed. The proposed inverse technique demonstrates very good results in simulation experiments, in particular, when the sensor array size is larger than the size of the object array.

2. STANDARD MODELS OF WAVEFIELD PROPAGATION

The object plane is a source of light radiation/reflection propagating along the axis z. The image plane is parallel to the object-plane with a distance z between the planes (see one of the typical setups in Fig. 1).

Let $u_z(x,y)$ be a complex-valued $2D$ wavefield defined in the $3D$ space (x,y,z) as a function of the lateral x, y and axial z variables. According to the scalar diffraction theory there is a linear operator which links the $2D$ wavefield distribution propagating along the axis z with the object wavefield $u_0(x,y)$ at $z=0$ as $u_z(x,y)=\mathcal{D}_z\{u_0(x,y)\}$, where $\mathcal{D}_z$ stands for a diffraction operator with a distance parameter z. The mathematical theory of this operator representation can be found in [3], where it is shown, in particular, that the diffraction operator can be given as an integral convolution

$$u_z(x,y)=\int\int g_z(x-\xi,y-\eta)u_0(\xi,\eta)d\xi d\eta,\ z>0. \quad (1)$$

The kernel g_z is shift invariant and has a form of the first Raylegh-Sommerfeld solution of the Maxwell-Helmholtz equation $\nabla^2 u+k^2u=0$, where the wavenumber $k=2\pi/\lambda$ and λ is a wavelength. This kernel is of the form $g_z=z\dfrac{\exp(j2\pi r/\lambda)}{j\lambda\cdot r^2}$, $r=\sqrt{x^2+y^2+z^2}$, $z\geq 0$, [4]. It is shown in [3] that the operator $\mathcal{D}_z$ is invertible and also can be presented as convolution with a shift-invariant kernel. If the diffraction

This work was supported by the Academy of Finland, project No. 213462 (Finnish Centre of Excellence program 2006 – 2011) and by EC within FP6 (Grant 511568 with the acronym 3DTV).

distribution $u_z(x,y)$ is given at the output image plane, the input object distribution at $z=0$ can be reconstructed using the inverse operator $\mathcal{D}_z^{-1}$, i.e. $u_0(x,y)=\mathcal{D}_z^{-1}\{u_z(x,y)\}$.

One of the fundamental results of the scalar diffraction theory is that the $2D$ integral Fourier transform of the kernel g_z has a form [3], [4]

$$G_z(\omega_x,\omega_y)=\mathcal{F}\{g_z(x,y)\}= \quad (2)$$
$$e^{j2\pi\frac{z}{\lambda}\sqrt{1-(\lambda\omega_x)^2-(\lambda\omega_y)^2}},\ (\omega_x,\omega_y)\in D_\lambda.$$

Thus, the diffraction operator with the kernel g_z is a low-pass filter with a non-zero transfer function on the disc $(\lambda\omega_x)^2+(\lambda\omega_y)^2<1$, with $|G_z|=1$ and the phase $\psi_{G_z}=2\pi\frac{z}{\lambda}\sqrt{1-(\lambda\omega_x)^2-(\lambda\omega_y)^2}$. Here ω_x and ω_y are frequencies in Hz and the disc $D_\lambda=\{(\omega_x,\omega_y):(\lambda\omega_x)^2+(\lambda\omega_y)^2<1\}$ defines the area where the transfer function G_z of the operator $\mathcal{D}_z$ is non-zero.

Note that, $G_z^*(\omega_x,\omega_y)=G_{-z}(\omega_x,\omega_y)$, then the forward and inverse frequency domain transforms are of the form

$$U_z(\omega_x,\omega_y)=G_z(\omega_x,\omega_y)U_0(\omega_x,\omega_y), \quad (3)$$
$$U_0(\omega_x,\omega_y)=G_{-z}(\omega_x,\omega_y)U_z(\omega_x,\omega_y), \quad (4)$$

where $U_z(\omega_x,\omega_y)=\mathcal{F}_{x,y}\{u_z(x,y)\}=\int\int u_z(x,y)e^{-j2\pi(\omega_x x+\omega_y y)}dxdy$.

If the spectrums $U_z(\omega_x,\omega_y)$, $U_0(\omega_x,\omega_y)$ are given the corresponding wavefields are calculated by the inverse Fourier transform, for instance

$$u_z(x,y)=\int\int U_z(\omega_x,\omega_y)e^{j2\pi(\omega_x x+\omega_y y)}d\omega_x d\omega_y. \quad (5)$$

Discretization of the integrals in the formulas (1), (5) is a standard idea to derive a discrete model for the wavefield propagation. It is well known that this problem is far from been trivial. The principal difficulty of discretization in the spatial domain (1) follows from the fact that the kernel g_z is modulated by a high-frequency harmonic factor $\exp(j2\pi r/\lambda)$. The discrete sampling of the rate at least twice higher than the highest frequency component of the integrand is a standard remedy. Obviously it can result in an unacceptably high sampling rate.

The discrete modeling of the diffraction transform is a subject of many publications. The review of this area is far beyond the scope of this paper. However, we wish to mention that the discrete space domain modelling for holography is discussed in details in [1] and the accuracy of the frequency domain approach is analyzed in [5].

The standard practical discrete models based on the fast Fourier transform (FFT) are obtained from the continuous domain representations (3)-(4). Let the object and image planes be square of $N_0\times N_0$, $N_z\times N_z$ pixels with the pixel's size $\Delta_0\times\Delta_0$ and $\Delta_z\times\Delta_z$ for the object and image planes, respectively.

If $N_0=N_z=N$ and $\Delta_0=\Delta_z=\Delta$, then the so-called convolution based discrete model is obtained from (3)-(4), where FFT is used instead of the integral Fourier transform (e.g. [1], [6]):

$$\bar{U}_z(f_x,f_y)=\bar{G}_z(f_x,f_y)\bar{U}_0(f_x,f_y), \quad (6)$$
$$\bar{U}_0(f_x,f_y)=\bar{G}_z^*(f_x,f_y)\bar{U}_z(f_x,f_y), \quad (7)$$

where $\bar{U}_z=\mathcal{FFT}\{u_z\}$, $\bar{U}_0=\mathcal{FFT}\{u_0\}$ and $\bar{G}_z=\mathcal{FFT}\{g_z\}$ are calculated over the arrays of the size $N\times N$.

3. DISCRETE DIFFRACTION TRANSFORM

Motivation for a discrete model developed in this paper is different from a direct integration of the space domain (1) or frequency domain (5) propagation equations. First, we assume that the input of our model is discrete defined by a pixel-wise constant object distribution and the output is also discrete as defined by outputs of sensor's pixels. A pixel-wise constant object distribution means that a distribution as a continuous variable function is invariant inside of pixels. Under this assumption we integrate the propagation equation (1) and arrive to the discrete-to-discrete modeling where the inputs are pixel values of the object distribution and the output are the pixel values of the sensor output.

We name this discrete model *discrete diffraction transform* (DDT). It can be presented in spatial and frequency domains. The following formulas are derived assuming that $\Delta_o=\Delta_z=\Delta$, while the sizes of the object and images arrays can be different, $N_z\lessgtr N_0$.

In the spatial domain DDT is a form:

$$u_z[k,l]=\sum_{s,t=-N_0/2}^{N_0/2-1}a_z[k-s,l-t]u_0[s,t],\ z>0, \quad (8)$$

where the kernel

$$a_z[k,l]=\frac{1}{\Delta^2}\int_{-\Delta/2}^{\Delta/2}\int_{-\Delta/2}^{\Delta/2}\int_{-\Delta/2}^{\Delta/2}\int_{-\Delta/2}^{\Delta/2} \quad (9)$$
$$g_z(k\Delta+\xi'+\xi,\ l\Delta+\eta'+\eta)d\xi d\eta d\xi' d\eta',$$
$$k,l=-N_a/2,...,N_a/2-1, \quad (10)$$
$$N_a=N_z+N_0-1. \quad (11)$$

FFT cannot be used directly for calculation of the convolution (8) even when $N_0=N_z=N$ because while the input u_0 and output u_z have the same size $N\times N$ the support size of the kernel a_z is much larger $(2N-1)\times(2N-1)$.

In order to make FFT applicable we use zero-padding of the variables u_0 and u_z extended to the extended size $N_a\times N_a$, covering the support of the kernel a_z. In what follows the wave-tilde ($\tilde{}$) means the corresponding variables extended by zero-padding to the size $N_a\times N_a$. The proposed frequency domain algorithm works with these extended size variables and exploits the advantage of FFT for fast and accurate calculation of the convolution (8).

The *frequency domain* calculation of DDT is produced according the following four step algorithm:

- Define FFT for u_0 extended to the size $N_a\times N_a$

$$\tilde{U}_0(f_x,f_y)=\mathcal{FFT}\{\tilde{u}_0\}= \quad (12)$$
$$\sum_{k,l=-N_0/2}^{N_0/2-1}u_0[k,l]W^{f_x k}W^{f_y l}=$$
$$\sum_{k,l=-N_a/2}^{N_a/2-1}\tilde{u}_0[k,l]W^{f_x k}W^{f_y l},$$
$$W=\exp(-j2\pi/(2N_a)),$$
$$f_x,f_y=-N_a/2,...,N_a/2-1,$$

- Calculate the transfer function of DDT

$$\tilde{A}_z(f_x,f_y)=\mathcal{FFT}\{\tilde{a}_z\}= \sum_{u,v=-N_a/2}^{N_a/2-1}\tilde{a}_z(u,v)W^{f_x u}W^{f_y v}, \quad (13)$$

- Calculate FFT for u_z extended to the size $N_a\times N_a$

$$\tilde{U}_z(f_x,f_y)=\tilde{A}_z(f_x,f_y)\tilde{U}_0(f_x,f_y), \quad (14)$$
$$\tilde{u}_z[k,l]=\mathcal{FFT}^{-1}\{\tilde{U}_z(f_x,f_y)\},$$
$$k,l=-N_a/2,...,N_a/2-1$$

- Calculate u_z of the original size $N_0\times N_0$

$$u_z(k,l)=\tilde{u}_z[k,l],\ k,l=-N_0/2,...,N_0/2-1. \quad (15)$$

Let us derive the above formulas. Assume that the distribution u_0 allows a pixel-wise constant approximation, then the integral (1) can be represented as

$$u_z(x,y)=\sum_{s,t=-N_0/2}^{N_0/2-1}u_0[s,t]\times \quad (16)$$
$$\int_{-\Delta/2}^{\Delta/2}\int_{-\Delta/2}^{\Delta/2}g_z(x-s\Delta+\xi,y-t\Delta+\eta)d\xi d\eta,$$
$$u_0[s,t]=u_0(s\Delta_o+\xi,t\Delta_o+\eta),\ -\Delta/2\le\xi,\eta<\Delta/2,$$

where the sum is calculated over the square array of $N_0\times N_0$ pixels of the size $\Delta\times\Delta$.

Let the output signal of any sensor's pixel be the mean value of the impinging distribution calculated as

$$u_z[k,l]=\frac{1}{\Delta^2}\int_{-\Delta/2}^{\Delta/2}\int_{-\Delta/2}^{\Delta/2}u_z(k\Delta+\xi,l\Delta+\eta)d\xi d\eta. \quad (17)$$

Inserting (16) into (17) we arrive to the model (8)-(10).

Thus, a_z is a smoothed (averaged) version of the original kernel g_z. The averaging in (9) takes into consideration discretization for both object and sensors arrays. For a pixel-wise constant object distribution u_0 the model (8)-(9) is accurate, i.e. gives the precise distribution for the image plane regardless conventional requirements concerning the digital integration for (1).

The frequency domain DDT (12)-(15) exploits the advantage of the fast Fourier transform (FFT) for accurate calculation of the convolution (8). The arguments of the kernel a_z in (8) belongs to the interval $[-N_a/2, N_a/2-1]$. In order to preserve the accurate result for $u_z[k,l]$ in (8) when FFT is used we extend the size $N_0\times N_0$ of the input array and the size $N_z\times N_z$ of the output arrays by the zero-padding to the size of the extended interval $[-N_a/2, N_a/2-1]$ and define the equation (8) for this larger area of k and l. Then, routine manipulations show that the formulas (12)-(15) give the result identical to (8).

The DDT is different from the integral counterparts in two important aspects: it accurately takes into consideration the finite size of the sensor and as a result it becomes ill-conditioned.

The DDT model is originated from [2], where it is introduced for $N_z=N_0$. In this paper we extend this approach to a more general case $N_z\gtrless N_0$ and show that larger values of $N_z>N_0$ are able to improve the accuracy of wavefield reconstruction.

In our implementation of (9) we exploit the Fresnel approximation of the kernel g_z

$$g_z\simeq\frac{\exp(j2\pi z/\lambda)}{j\lambda\cdot z}\exp[j\frac{\pi}{\lambda z}(x^2+y^2)]. \quad (18)$$

Then a_z can be written as

$$a_z[k,l]\simeq\frac{\exp(j2\pi z/\lambda)}{j\lambda\cdot z}\rho_{z,\lambda}[k]\rho_{z,\lambda}[l],$$

where $\rho_{z,\lambda}[k]=\frac{1}{\Delta}\int_{-\Delta/2}^{\Delta/2}\int_{-\Delta/2}^{\Delta/2}\exp(j\frac{\pi}{\lambda z}(k\Delta+\xi'+\xi)^2)d\xi d\xi'=2\int_{-\Delta}^{\Delta}(1-\frac{|v|}{\Delta})\exp(j\frac{\pi}{\lambda z}(k\Delta+v)^2)dv$.

4. DIGITAL HOLOGRAM FORMATION

The basic setup for the in-line phase-shifting holography is presented in Fig. 1. The object beam and the reference beam reflected at the piezoelectric transducer mirror controlled by a computer are combined at the digital sensor and form interference pattern [1], [6]. At least three records of this pattern are acquired which are different by the phase-shifts of the reference beam. The wavefield impinging on the sensor can be presented in the form

$$I_\phi(x,y)=|u_z(x,y)+u_{ref}(x,y)e^{j\phi}|^2=$$
$$|u_z(x,y)|^2+|u_{ref}(x,y)|^2+$$
$$u_z(x,y)u_{ref}(x,y)e^{j\phi(x,y)}+u_z^*(x,y)u_{ref}^*(x,y)e^{-j\phi(x,y)}.$$

Assume for simplicity that u_{ref} and the phase shift are invariant then the outputs of the sensor pixel are calculated according to (17) as

$$I_\phi[k,l]=I_z[k,l]+|u_{ref}|^2+ \quad (19)$$
$$u_z[k,l]u_{ref}e^{j\phi}+u_z^*[k,l]u_{ref}^*e^{-j\phi},$$

where

$$I_\phi[k,l]=\frac{1}{\Delta^2}\int_{-\Delta/2}^{\Delta/2}\int_{-\Delta/2}^{\Delta/2}I_\phi(k\Delta+\xi,l\Delta+\eta)d\xi d\eta,$$
$$I_z[k,l]=\frac{1}{\Delta^2}\int_{-\Delta/2}^{\Delta/2}\int_{-\Delta/2}^{\Delta/2}|u_z(k\Delta+\xi,l\Delta+\eta)|^2d\xi d\eta,$$

and $u_z[k,l]$ are given by (8).

Let us use for the phase shift $\phi=0,\pi/2,\pi$ then it follows from (19) that the wavefield $u_z[k,l]$ can be calculated as

$$u_z[k,l]=\frac{1}{4u_{ref}}(I_0-I_\pi-j(2I_{\pi/2}-I_0-I_\pi)) \quad (20)$$

and the wavefield reconstruction is reduced to reconstruction of the discrete object distribution $u_0[k,l]$ from the wavefield distribution $u_z[k,l]$ given in the sensor plane.

5. DDT HOLOGRAM RECONSTRUCTION

Reconstruction of the $2D$ object wavefield u_0 from u_z is a discrete inverse problem. The model (8) can be rewritten in the vector form $\mathbf{u}_z = \mathcal{A}_z \cdot \mathbf{u}_0$, where $\mathbf{u}_z \in R^{N_z^2}$ and $\mathbf{u}_0 \in R^{N_0^2}$ are vectors formed from $u_z[k,l]$ and $u_0[k,l]$, respectively, and the $\mathcal{A}_z$ matrix $N_z^2 \times N_0^2$ is formed from $a_z[k,l]$. If $\mathcal{A}_z$ is a full rank matrix and $N_z \geq N_0$ a perfect reconstruction of $\mathbf{u}_0$ from $\mathbf{u}_z$ is possible. However, for usual sensor sizes (say 512×512 or 1024×1024) the dimension of this space domain model becomes too high for practical calculations for both the forward prediction of $\mathbf{u}_z$ from $\mathbf{u}_0$ and the backward inverse with reconstruction of $\mathbf{u}_0$ from $\mathbf{u}_z$. We use the frequency domain DDT in order to obtain an approximate simple solution.

Assume that $\tilde{U}_z(f_x, f_y)$ in (14) is given and introduce the following quadratic criterion

$$J = ||\tilde{U}_z - \tilde{A}_z \tilde{U}_0||^2 + \alpha ||\tilde{U}_0||^2, \tag{21}$$

where the Euclidean norm $||\cdot||^2$ is calculated over the frequencies f_x, f_y, for instance $||\tilde{U}_0||^2 = \sum_{f_x,f_y} |\tilde{U}_0(f_x,f_y)|^2$, and $\alpha > 0$ is a regularization parameter,

Minimization of J with respect to $\tilde{U}_0$ gives the minimum condition in the form $\partial J / \partial \hat{U}_0^* = 0$ and the following solution

$$\hat{U}_0 = \tilde{A}_z^* \cdot \tilde{U}_z / (|\tilde{A}_z|^2 + \alpha^2), \tag{22}$$

$$\tilde{u}_0 = \mathcal{F}\mathcal{F}\mathcal{T}^{-1}\{\hat{U}_0\},$$

$$\hat{u}_0[k,l] = \tilde{u}_0[k,l],\ k,l = -N_0/2, ..., N_0/2-1. \tag{23}$$

Here $\hat{u}_0$ is the regularized inverse estimate of the object wavefield distribution. The parameter $\alpha > 0$ controls a level of smoothing in the regularized inverse. The extended $N_a \times N_a$ size frequency characteristic $\hat{U}_z$ in (22) is calculated from the zero-padded sensor registered data u_z of the size $N_z \times N_z$.

It is assumed in our experiments that the sensor size is equal to $\Delta \cdot N_0 = 0.01\ m$. The frequency of the varying on x harmonic factor $\exp[j\frac{\pi}{\lambda z}(x^2+y^2)]$ of the kernel (18) is calculated as $2\pi x/\lambda z$. The maximum values of x is equal to half of the sensor linear size, $x_{\max} = 0.01/2 = 0.005\ m$. Then the upper bound for the frequency is equal to $2\pi x_{\max}/\lambda z$. For the wavelength $\lambda = 0.632\ \mu m$, $N_0 = 512$ and $\Delta = 0.01/512$ the Nyquist requirement for the non-alising sampling follows from the inequality $2\pi x_{\max}/\lambda z < \pi/\Delta$, i.e. $z > z_{crit} = 2\Delta x_{\max}/\lambda = 0.309\ m$.

In the presented simulation results we assume that $z = 0.15\ m$, i.e. the Nyquist condition is violated. The set of images in Fig.2 - Fig.4 shows the object distribution reconstruction for the test image *Baboon* (512×512) produced for $N_z = N_0$ and for the larger sensor size $N_z = 1.5 \cdot N_0 = 768$. The regularization parameter is selected experimentally as $\alpha = 0.01$ fixed in all experiments.

In this modelling the *Baboon* test image defines the phase $u^{\#}[k,l]$ of the object distribution assuming that the amplitude is equal to 1, $u_0[k,l] = \exp(-j\pi(u^{\#}[k,l] - .5))$. The phase of $u_0[k,l]$ takes values in the segment $[-.5, 0.5]$,

The observed complex-valued wavefield (768×768) is shown in the first two images in Fig.2. The last image in Fig.2 shows the phase reconstruction obtained using the standard convolution based FFT algorithm (7). This reconstruction completely fails with a periodical disturbance pattern typical for the aliasing effects destroying the image beyond recognition.

The results for the DDT reconstructions are shown in Fig.2 and Fig.3 for the phase and amplitude of the wavefield. The quality of imaging becomes much better for the larger sensor size with nearly perfect reconstruction for the sensor of the size $1.5 \cdot N_0 = 768$. This improvement in performance is illustrated by root-mean-squared-error ($RMSE$) shown in the images. The module estimates in Fig.4 also shows the estimate improvement when the sensor size becomes larger. The true module in the object plane is invariant and equal to 1 and we can note that for the larger N_z the module estimate is indeed nearly invariant in lateral coordinates x, y.

The standard algorithm fails for small distances $z < z_{crit}$, however it works for a larger distances $z > z_{crit}$ with a definite visual and numerical accuracy advantage of the proposed DDT based algorithm. In these experiments the simulated observations are accurate because the forward DDT gives the accurate results for any pixel-wise constant object distribution. The used test image defined on the 512×512 array gives an example of this sort of pixel-wise invariant distributions. Thus, the produced comparison of the FFT and novel DDT based algorithms is quite accurate despite the fact that it is given by simulation only.

Similar experiments for a number of test images with amplitude and phase modulation of the object distribution have been produced and showed the visual and accuracy advantage of the DDT algorithm with respect to the considered standard convolution based FFT algorithm.

6. CONCLUSION

A novel discrete model for forward wavefield propagation is proposed. This model is accurate for a pixel-wise constant object distribution. A wavefield reconstruction for phase-shifting holography is considered as a discrete inverse problem. For the inverse we use the regularized frequency domain technique. It is shown that a larger size of the sensor results in an essential imaging improvement.

REFERENCES

[1] Th.Kreis, *Handbook of Holographic Interferometry (Optical and Digital Methods)*, Wiley-VCH Gmbh&Co.KGaA, Weinheim, 2005.

[2] V. Katkovnik, J. Astola, K. Egiazarian, "Wavefield reconstruction and design as discrete inverse problems," *Proceedings 3D TV Conference*, Istanbul, Turkey, 2008.

[3] G. S. Sherman, "Integral-transform formulation of diffraction theory," *J. Opt. Soc. Am*, vol. 57, n^{0}12, pp. 1490-1498, 1967.

[4] J. W. Goodman, *Introduction to Fourier Optics*, McGraw-Hill, Inc, New York, Second Edition, 1996.

[5] L. Onural, "Exact analysis of the effects of sampling of the scalar diffraction field," *J. Opt. Soc. Am. A,* vol. 24, no. 2, pp. 359-367, 2007.

[6] I. Yamaguchi, J. Kato, S. Ohta, and J. Mizuno, "Image formation in phase-shifting digital holography and applications to microscopy," *Appl. Opt.*, vol. 40, no. 34, 6177–6186, 2001.

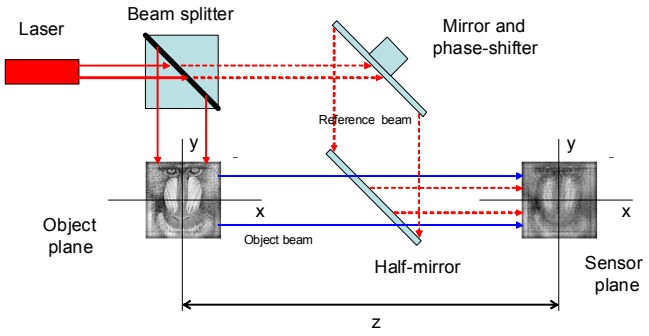

Figure 1: Principal setup of phase-shifting digital holography.

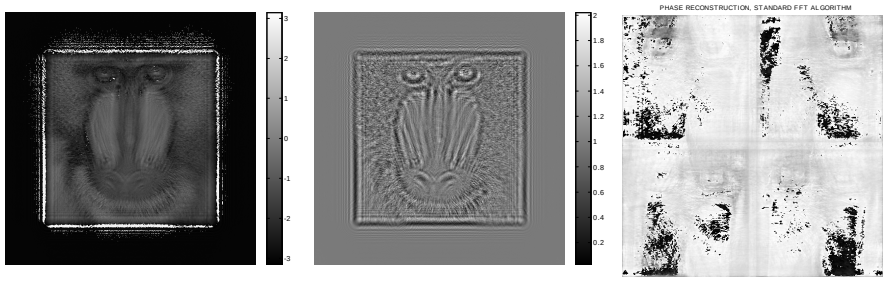

Figure 2: The first two images (768 × 768) are phase and module observations at the sensor plane, respectively. The last image (512 × 512) is a phase reconstruction obtained by the standard convolution FFT algorithm. It is disturbed beyond recognition of the test image, i.e. this algorithm fails.

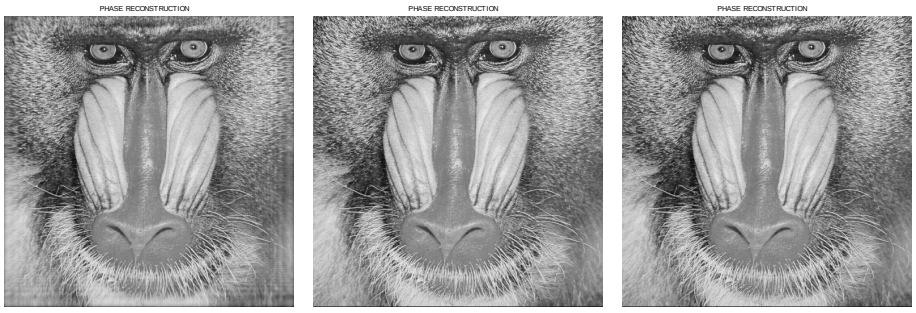

Figure 3: The phase of the object distribution reconstruction with different sensor size: (a) 512 × 512, $RMSE = 0.035$; (b) 768 × 768, $RMSE = 0.0059$; (c) 1024 × 1024, $RMSE = 0.0057$.

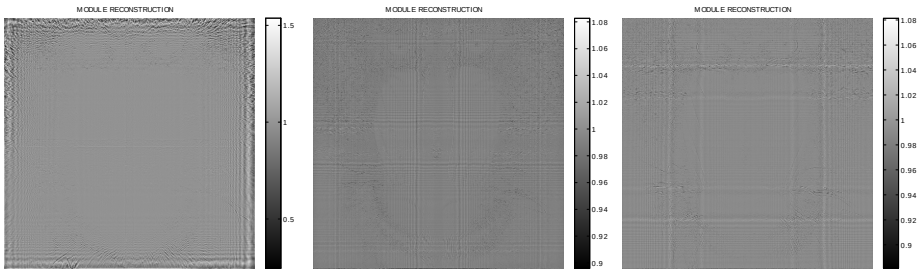

Figure 4: The module of the object distribution reconstruction with different sensor size: (a) 512 × 512, (b) 768 × 768, (c) 1024 × 1024.